Electron-phonon coupling and electron self-energy in electron-doped graphene: Calculation of angular-resolved photoemission spectra

Matteo Calandra and Francesco Mauri
CNRS and Institut de Minéralogie et de Physique des Milieux condensés, case 115, 4 place Jussieu, 75252, Paris cedex 05, France
(Received 16 May 2007; published 9 November 2007)

We obtain analytical expressions for the electron self-energy and the electron-phonon coupling in electron-doped graphene using electron-phonon matrix elements extracted from density functional theory simulations. From the electron self-energies we calculate angle-resolved photoemission spectra (ARPES). We demonstrate that the measured kink at ≈ -0.2 eV from the Fermi level is actually composed of two features, one at ≈ -0.195 eV due to the twofold-degenerate E_{2g} mode, and a second one at ≈ -0.16 eV due to the A_1' mode. The electron-phonon coupling extracted from the kink observed in ARPES experiments is roughly a factor of 5.5 larger than the calculated one. This disagreement can be only partially reconciled by the inclusion of resolution effects. Indeed, we show that a finite resolution increases the apparent electron-phonon coupling by underestimating the renormalization of the electron velocity at energies larger than the kink positions. The discrepancy between theory and experiments is thus reduced to a factor of ≈ 2.5. From the linewidth of the calculated ARPES we obtain the electron relaxation time. A comparison with available experimental data in graphene shows that the electron relaxation time detected in ARPES is almost two orders of magnitudes smaller than that measured by other experimental techniques.

DOI: 10.1103/PhysRevB.76.205411 PACS number(s): 79.60.−i, 74.25.Jb, 71.15.Mb, 74.25.Kc

I. INTRODUCTION

The recent experimental realization of a single graphene monolayer has allowed the study of the electronic structure of a two-dimensional (2D) electron system with Dirac-like dispersion.[1] Despite the fact that the band structure of graphene is calculated in many solid-state textbooks,[2,3] its experimental verification has been provided only recently by angular-resolver photoemission spectroscopy (ARPES) measurements on a graphene monolayer deposed on a SiC substrate.[4–6] The peculiar features of the electronic structure predicted theoretically are qualitatively confirmed by experiments: the carbon π bands (i) cross at the K point in the Brillouin zone (Dirac point) and (ii) depart linearly with a slope v_f from the Dirac point; (iii) the Fermi velocity extracted from experiments[5] is slightly larger (10–20%) than that calculated theoretically using density functional theory (DFT).

In addition to this encouraging agreement between theory and experience, recent angular photoemission experiments[6,7] performed on graphene revealed remarkable surprises. Two kinks are seen in the ARPES dispersion: the first one is at energies of 0.2 eV below the Fermi level (ϵ_f) and its energy position with respect to ϵ_f is unchanged as a function of the doping level, while the second one is closer to the Dirac point and its energy position with respect to ϵ_f decreases rapidly as the doping level is increased (see Fig. 2 in Ref. 6). The first kink has been attributed to a phonon feature,[6] while the second kink has been interpreted as due to a plasmon.[6,8] In what follows we focus on the first kink.

The ARPES momentum distribution curves (MDCs) associated with the −0.2 eV kink display a puzzling behavior as a function of doping. Indeed, it is observed that the magnitude of the jump associated with the MDC linewidth in the $-0.5 < \epsilon - \epsilon_f < 0$ eV energy window decreases as a function of doping (see Fig. 3 in Ref. 6, where from top to bottom the jump increases). This is surprising since, if this jump is associated with the electron-phonon interaction, then it should reflect the imaginary part of the electron self-energy due to the electron-phonon interaction. Since the magnitude of this interaction is usually proportional to the density of states at the Fermi level, the jump should increase as the doping level is increased. Thus the opposite behavior should be expected. This contradiction can be solved by noting that at low doping the tail of the second peak (attributed to a plasmon) is fairly close in energy and could affect the low-energy part of the momentum distribution curve. At larger dopings[9] the plasmon peak has no effect, and the electron-phonon coupling does increase as a function of doping. Thus we focus in the doping region identified by $\epsilon_f > 0.3$ eV (the energy zero being at the Dirac point).

In this work, we calculate the electron-phonon coupling parameter and the electron-phonon coupling contribution to the electron self-energy in doped graphene. In particular, we give an explicit demonstration of Eq. (1) in Ref. 10. From the electron self-energy we obtain the spectral-weight function and the ARPES spectra. Finally, we compare the calculated spectra with available experimental data, discussing in detail the important finite-resolution effects.

The paper is structured as follows. In Sec. II we obtain an analytical expression for the electron-phonon coupling in doped graphene. The electron self-energy is calculated in sec. III. The ARPES spectra are calculated from the electron self-energy in Sec. IV, including finite-resolution effects. Finally, in Sec. V we compare the electron relaxation time measured by different experimental techniques for both electron-doped graphene and graphite. Section VI is devoted to conclusions.

II. ELECTRON-PHONON COUPLING IN DOPED GRAPHENE

The 2D volume of the graphene Brillouin-zone (BZ) is $\Omega = (2/\sqrt{3})(2\pi/a)^2$ with $a = 2.46$ Å. The graphene π^* bare

bands (in the absence of electron-phonon coupling) are linear with slope $\beta=\hbar v_f=5.52$ eV Å (within DFT) close to the Dirac points $\mathbf{K}=(1/3,1/3,0)2\pi/a$ and $\mathbf{K}'=2\mathbf{K}$. The density of states per spin at a general energy ϵ above or below the Dirac point, but still in the region where the π^* bands can be considered linear, can thus be written as

$$N_\sigma(\epsilon)=\frac{a^2\sqrt{3}|\epsilon|}{2\pi\beta^2}=\frac{4\pi|\epsilon|}{\Omega\beta^2}. \tag{1}$$

Note that in this work energies are always measured with respect to the Dirac point.

The electron-phonon coupling for a mode ν at momentum $\mathbf{q}$ due to the π^* bands in graphene is given by

$$\lambda_{\mathbf{q}\nu}=\frac{2}{\hbar\omega_{\mathbf{q}\nu}N_\sigma(\epsilon_f)}\int_{\mathrm{BZ}}\frac{d\mathbf{k}}{\Omega}|g^{\nu}_{\mathbf{k}\pi^*\mathbf{k}+\mathbf{q}\pi^*}|^2 \times\delta(\epsilon_{\mathbf{k}}-\epsilon_f)\delta(\epsilon_{\mathbf{k}+\mathbf{q}}-\epsilon_f), \tag{2}$$

where $\omega_{\mathbf{q}\nu}$ is the phonon frequency of the mode ν at momentum $\mathbf{q}$ and $g^{\nu}_{\mathbf{k}\pi^*\mathbf{k}+\mathbf{q}\pi^*}$ is the electron-phonon matrix element for the π^* band $\epsilon_{\mathbf{k}}$ and for the phonon mode ν.

To illustrate how the integral is evaluated, we introduce the following two regions of space, namely, the sets

$$\mathcal{F}_{\mathbf{K}}(\epsilon)=\{\mathbf{k}|\ \beta|\mathbf{k}-\mathbf{K}|<\epsilon+\eta\}, \tag{3}$$

$$\mathcal{F}_{\mathbf{K}'}(\epsilon)=\{\mathbf{k}|\ \beta|\mathbf{k}-\mathbf{K}'|<\epsilon+\eta\}. \tag{4}$$

In these definitions, η is a small positive quantity. For $\epsilon=\epsilon_f$, since we assume that the Fermi level is not too far from the Dirac point so that the π^* bands are linear, $|\mathbf{k}-\mathbf{K}|$ or $|\mathbf{k}-\mathbf{K}'|$ is a small but finite vector and $\mathcal{F}_{\mathbf{K}}(\epsilon_f)\cap\mathcal{F}_{\mathbf{K}'}(\epsilon_f)$ is empty. The boundary of each region of space at $\eta=0$ (circumference) is indicated as $\partial\mathcal{F}_{\mathbf{K}}(\epsilon_f)$ and $\partial\mathcal{F}_{\mathbf{K}'}(\epsilon_f)$.

In Eq. (2), the two δ functions restrict the $\mathbf{k}$ integrations to the region of space satisfying the conditions $\epsilon_{\mathbf{k}}=\epsilon_f$ and $\epsilon_{\mathbf{k}+\mathbf{q}}=\epsilon_f$. The set of $\mathbf{k}$ points such that $\epsilon_{\mathbf{k}}=\epsilon_f$ is composed by the set $\partial\mathcal{F}_{\mathbf{K}}(\epsilon_f)\cup\partial\mathcal{F}_{\mathbf{K}'}(\epsilon_f)$. Thus, in the integral in Eq. (2), two cases are given (labeling $\mathbf{k}'=\mathbf{k}+\mathbf{q}$): (i) $\mathbf{k},\mathbf{k}'\in\partial\mathcal{F}_{\mathbf{K}}(\epsilon_f)$ or $\mathbf{k},\mathbf{k}'\in\partial\mathcal{F}_{\mathbf{K}'}(\epsilon_f)$, and (ii) $\mathbf{k}\in\partial\mathcal{F}_{\mathbf{K}}(\epsilon_f)$, $\mathbf{k}'\in\partial\mathcal{F}_{\mathbf{K}'}(\epsilon_f)$, or vice versa.

In case (i), scattering occurs at $\mathbf{q}=\mathbf{\Gamma}+\tilde{\mathbf{q}}$, with small $\tilde{\mathbf{q}}$, and π^* bands can only couple to the twofold-degenerate E_{2g} phonon mode. In case (ii), scattering occurs at $\mathbf{q}=\mathbf{K}+\tilde{\mathbf{k}}$ or at $\mathbf{q}=\mathbf{K}'+\tilde{\mathbf{k}}$, with small $\tilde{\mathbf{k}}$, and the π^* bands can only couple to the A_1' phonon mode.[11] The electron-phonon matrix elements involved in the two scattering process have been fitted to *ab initio* data in Ref. 11 and are

$$|g^{E_{2g}}_{\mathbf{K}+\tilde{\mathbf{k}}\pi^*,\mathbf{K}+\tilde{\mathbf{k}}+\tilde{\mathbf{q}}\pi^*}|^2=\langle g^2_{\mathbf{\Gamma}}\rangle[1\pm\cos(\theta_{\tilde{\mathbf{k}},\tilde{\mathbf{q}}}+\theta_{\tilde{\mathbf{k}},\tilde{\mathbf{k}}+\tilde{\mathbf{q}}})], \tag{5}$$

$$|g^{A_{1'}}_{\mathbf{K}+\tilde{\mathbf{k}}\pi^*,\mathbf{K}'+\tilde{\mathbf{k}}+\tilde{\mathbf{q}}\pi^*}|^2=\langle g^2_{\mathbf{K}}\rangle[1-\cos(\theta_{\tilde{\mathbf{k}},\tilde{\mathbf{k}}+\tilde{\mathbf{q}}})]. \tag{6}$$

In Eq. (5) + (−) sign refers to the LO (TO) E_{2g} mode, respectively, $\langle g^2_{\mathbf{\Gamma}}\rangle=0.0405$ eV^2, $\langle g^2_{\mathbf{K}}\rangle=0.0994$ eV^2, and $\theta_{\mathbf{u},\mathbf{v}}$ is the minimal angle between the two vectors $\mathbf{u},\mathbf{v}$.

For case (i) one has

$$\lambda_{\tilde{\mathbf{q}}E_{2g}}=\frac{2\times2\times2\langle g^2_{\mathbf{\Gamma}}\rangle_F}{\hbar\omega_{\tilde{\mathbf{q}}E_{2g}}N_\sigma(\epsilon_f)}\int_{\mathcal{F}_{\mathbf{\Gamma}}(\epsilon_f)}\frac{d^2\tilde{k}}{\Omega} \times\delta(\epsilon_{\mathbf{K}+\tilde{\mathbf{k}}}-\epsilon_f)\delta(\epsilon_{\mathbf{K}+\tilde{\mathbf{k}}+\tilde{\mathbf{q}}}-\epsilon_f)=\frac{8\langle g^2_{\mathbf{\Gamma}}\rangle_F}{\hbar\omega_{\tilde{\mathbf{q}}E_{2g}}N_\sigma(\epsilon_f)}I_{\tilde{\mathbf{q}}}, \tag{7}$$

where

$$\mathcal{F}_{\mathbf{\Gamma}}(\epsilon)=\{\mathbf{k}|\ \beta k<\epsilon+\eta\}. \tag{8}$$

The prefactor 8 is the result of having two E_{2g} modes and of having an identical integral over the second Fermi surface sheet at $\mathbf{K}'$. The integral $I_{\tilde{\mathbf{q}}}$ is the so-called nesting factor, defined as

$$I_{\tilde{\mathbf{q}}}=\int_{\mathcal{F}_{\mathbf{\Gamma}}(\epsilon_f)}\frac{d^2\tilde{k}}{\Omega}\delta(\epsilon_{\mathbf{K}+\tilde{\mathbf{k}}}-\epsilon_f)\delta(\epsilon_{\mathbf{K}+\tilde{\mathbf{k}}+\tilde{\mathbf{q}}}-\epsilon_f). \tag{9}$$

The electron-phonon coupling due to E_{2g} modes is given by

$$\lambda_{\mathbf{\Gamma}}(\epsilon_f)=\int_{\mathcal{F}_{\mathbf{\Gamma}}(2\epsilon_f)}\frac{d^2\tilde{q}}{\Omega}\lambda_{\tilde{\mathbf{q}}E_{2g}}=\frac{2\langle g^2_{\mathbf{\Gamma}}\rangle_F}{\hbar\omega_{\mathbf{\Gamma}E_{2g}}}, \tag{10}$$

where we have used the fact that

$$\int_{\mathcal{F}_{\mathbf{\Gamma}}(2\epsilon_f)}\frac{d^2\tilde{q}}{\Omega}I_{\tilde{\mathbf{q}}}=N^2_\sigma(\epsilon_f)/4, \tag{11}$$

and we have replaced the E_{2g} phonon frequency with its value at $\mathbf{\Gamma}$.

Similarly, case (ii) leads to

$$\lambda_{\mathbf{K}+\tilde{\mathbf{q}}A_1'}=\frac{2\times2\langle g^2_{\mathbf{K}}\rangle_F}{\hbar\omega_{\mathbf{K}+\tilde{\mathbf{q}}A_1'}N_\sigma(\epsilon_f)}\int_{\mathcal{F}_{\mathbf{K}}(\epsilon_f)}\frac{d^2\tilde{k}}{\Omega}[1-\cos(\theta_{\tilde{\mathbf{k}},\tilde{\mathbf{k}}+\tilde{\mathbf{q}}})] \times\delta(\epsilon_{\mathbf{K}'+\tilde{\mathbf{k}}}-\epsilon_f)\delta(\epsilon_{\mathbf{K}+\tilde{\mathbf{k}}+\tilde{\mathbf{q}}}-\epsilon_f) =\frac{4\langle g^2_{\mathbf{K}}\rangle_F}{\hbar\omega_{\mathbf{K}+\tilde{\mathbf{q}}A_1'}N_\sigma(\epsilon_f)}J_{\mathbf{K}+\tilde{\mathbf{q}}}, \tag{12}$$

and the additional factor of 2 is a result of having scattering from $\mathcal{F}_{\mathbf{K}}(\epsilon_f)$ to $\mathcal{F}_{\mathbf{K}'}(\epsilon_f)$ and vice versa. The quantity

$$J_{\mathbf{K}+\tilde{\mathbf{q}}}=\int_{\mathcal{F}_{\mathbf{K}}(\epsilon_f)}\frac{d^2\tilde{k}}{\Omega}[1-\cos(\theta_{\tilde{\mathbf{k}},\tilde{\mathbf{k}}+\tilde{\mathbf{q}}})] \times\delta(\epsilon_{\mathbf{K}'+\tilde{\mathbf{k}}}-\epsilon_f)\delta(\epsilon_{\mathbf{K}+\tilde{\mathbf{k}}+\tilde{\mathbf{q}}}-\epsilon_f) \tag{13}$$

and its integral over the momentum $\tilde{\mathbf{q}}$ are evaluated in Appendix A, so that the contribution of the A_1' mode to the electron-phonon coupling is

$$\lambda_{\mathbf{K}}(\epsilon_f)=\int_{\mathcal{F}_{\mathbf{K}}(2\epsilon_f)}\frac{d^2\tilde{q}}{\Omega}\lambda_{\mathbf{K}+\tilde{\mathbf{q}}A_1'}=\frac{\langle g^2_{\mathbf{K}}\rangle_F N_\sigma(\epsilon_f)}{\hbar\omega_{\mathbf{K}A_1'}}, \tag{14}$$

where we have approximated $\omega_{\mathbf{K}+\tilde{\mathbf{q}}A_1'}\approx\omega_{\mathbf{K}A_1'}$.

The total electron-phonon coupling is thus

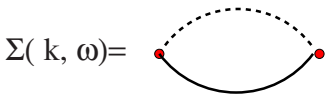

FIG. 1. (Color online) Lowest-order contribution to the electron self-energy due to the electron-phonon interaction. The dotted (continuous) line represents the phonon (electron) self-energy.

$$\lambda(\epsilon_f) = N_\sigma(\epsilon_f)\left(\frac{2\langle g^2_{\mathbf{\Gamma}}\rangle_F}{\hbar\omega_{\mathbf{\Gamma}E_{2g}}} + \frac{\langle g^2_{\mathbf{K}}\rangle_F}{\hbar\omega_{\tilde{\mathbf{q}}A_1'}}\right) \tag{15}$$

which is Eq. (1) in Ref. 10. Using numerical values of $\hbar\omega_{\mathbf{\Gamma}E_{2g}}=0.195$ eV and $\hbar\omega_{\mathbf{K}A_1'}=0.16$ eV, we get

$$\lambda(\epsilon_f) = N_\sigma(\epsilon_f)(1.04\ \text{eV}) = \frac{4\pi^{3/2}\sqrt{n}}{\Omega\beta}(1.04\ \text{eV}) = 5.55\sqrt{n} \times 10^{-9}\ \text{cm}, \tag{16}$$

where n is the number of electron per surface area.

III. ELECTRON SELF-ENERGY AND ANGLE-RESOLVED PHOTOEMISSION

The lowest contribution to the retarded electron self-energy due to coupling of π^* electrons to a phonon mode ν is illustrated in Fig. 1. At zero temperature direct calculation[12] of the diagram gives:

$$\Sigma_\nu(\mathbf{k},\epsilon) = \sum_{\alpha=\{-1,1\}} \int_{\mathrm{BZ}} \frac{d^2\mathbf{q}}{\Omega} |g^\nu_{\mathbf{k}\pi^*,\mathbf{k}+\mathbf{q}\pi^*}|^2 \times \left(\frac{\Theta(\alpha\epsilon_f - \alpha\epsilon_{\mathbf{k}+\mathbf{q}})}{\epsilon + i\delta - (\epsilon_{\mathbf{k}+\mathbf{q}}) + \alpha\hbar\omega_{\mathbf{q}\nu}}\right) \tag{17}$$

where $\Theta(x)$ is the Heaviside function. The imaginary part of Eq. (17) is

$$\begin{aligned}\Sigma''_\nu(\mathbf{k},\epsilon) &= -\pi \sum_{\alpha=\{-1,1\}} \int_{\mathrm{BZ}} \frac{d^2\mathbf{q}}{\Omega} |g^\nu_{\mathbf{k}\pi^*,\mathbf{k}+\mathbf{q}\pi^*}|^2 \\ &\quad \times \Theta(\alpha\epsilon_f - \alpha\epsilon_{\mathbf{k}+\mathbf{q}})\delta(\epsilon - \epsilon_{\mathbf{k}+\mathbf{q}} + \alpha\hbar\omega_{\mathbf{q}\nu}) \\ &= -\pi \sum_{\alpha=\{-1,1\}} \Theta(\alpha\epsilon_f - \alpha\epsilon - \hbar\omega_{\mathbf{q}\nu}) \\ &\quad \times \int_{\mathrm{BZ}} \frac{d^2\mathbf{k}'}{\Omega} |g^\nu_{\mathbf{k}\pi^*,\mathbf{k}'\pi^*}|^2 \delta(\epsilon - \epsilon_{\mathbf{k}'} + \alpha\hbar\omega_{\mathbf{k}'-\mathbf{k}\nu}).\end{aligned} \tag{18}$$

In angular-resolved photoemission experiments, the graphene is electron doped, so the Fermi level is larger than the Dirac point but it is still in the region where $\epsilon_{\mathbf{k}}$ can be considered linear. For a given mode ν and a given value of α, the δ function in Eq. (18) restricts the BZ integration to two regions, close to $\mathbf{K}$ and to $\mathbf{K}'$. The restriction to these regions of $\mathbf{k}$ space and the fact that we are interested in the region of energy-momentum close to the Dirac point, namely, $\mathbf{k}=\mathbf{K}+\tilde{\mathbf{k}}$ with $\tilde{\mathbf{k}}$ small, furthermore restricts the integration region. Indeed, it implies that for small $\tilde{\mathbf{q}}$ (i) $\mathbf{q}=\tilde{\mathbf{q}}$ and (ii) $\mathbf{q}=\mathbf{K}+\tilde{\mathbf{q}}$.

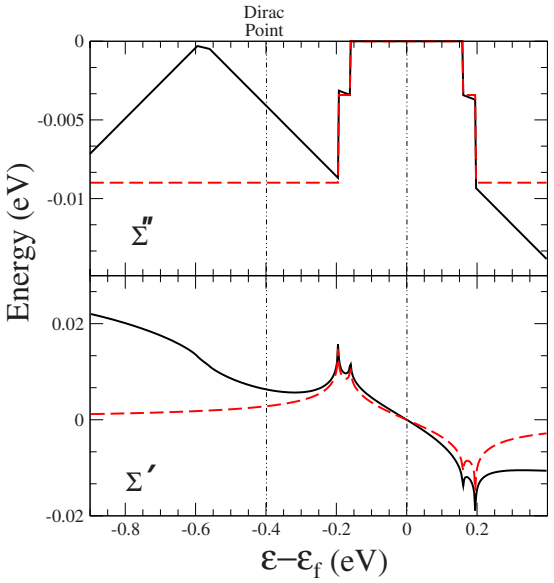

FIG. 2. (Color online) Real (Σ') and imaginary (Σ'') parts of the electron self-energy in graphene (continuous line). Dashed lines refer to self-energy parts obtained using a constant density of states. The Fermi level is $\epsilon_f=0.4$ eV.

Case (i) represents scattering to phonons close to the Γ point and (ii) to phonons close to the $\mathbf{K}$ point. So the situation is similar to the previous electron-phonon calculation.

The total self-energy $\Sigma''=\Sigma_{\nu=\{E_{2g},A_1'\}}\Sigma''_\nu$ due to the two E_{2g} phonon modes at $\mathbf{\Gamma}$ and to the A_1' phonon mode at $\mathbf{K}$ is obtained by substituting Eqs. (5) and (6) in Eq. (18), assuming a constant phonon dispersion around $\mathbf{\Gamma}$ and $\mathbf{K}$ and performing the integration over the BZ, as

$$\begin{aligned}\Sigma''(\tilde{\mathbf{k}},\epsilon) = -\frac{\pi}{2} \sum_{\alpha=\{-1,1\}} &[\hbar\omega_{\mathbf{\Gamma}E_{2g}}\lambda_{\mathbf{\Gamma}}(\epsilon - \alpha\hbar\omega_{\mathbf{\Gamma}E_{2g}}) \\ &\times \Theta(\alpha\epsilon_f - \alpha\epsilon - \hbar\omega_{\mathbf{\Gamma}E_{2g}}) + \hbar\omega_{\mathbf{K}A_1'}\lambda_{\mathbf{K}}(\epsilon - \alpha\hbar\omega_{\mathbf{K}A_1'}) \\ &\times \Theta(\alpha\epsilon_f - \alpha\epsilon - \hbar\omega_{\mathbf{K}A_1'})],\end{aligned} \tag{19}$$

where $\lambda_{\mathbf{\Gamma}}(\epsilon-\hbar\omega_{\mathbf{\Gamma}E_{2g}})$ and $\lambda_{\mathbf{K}}(\epsilon-\hbar\omega_{\mathbf{K}A_1'})$ are defined in Eqs. (10) and (14), respectively. From Eq. (19) we note that for small $\tilde{\mathbf{k}}$ the imaginary part of the phonon self-energy is momentum independent, so in what follows we drop the $\tilde{\mathbf{k}}$ label. $\Sigma''(\epsilon)$ is illustrated in Fig. 2 (black lines).

The imaginary part in Eq. (19) has to be compared with the square well model which is obtained from Eq. (19), assuming a constant density of states. This is the commonly used approximation to interpret ARPES spectra.[13,14] The square well model is illustrated in Fig. 2 [red (dashed) line]. In graphene this approximation is in principle not allowed because the density of states is proportional to $|\epsilon|$ [see Eq. (1)]. The difference between the two models becomes relevant for energies smaller than or close to the Dirac point.

The real part of the electron self-energy can be obtained using the Kramers-Kronig relations, namely,

$$\Sigma'(\epsilon) = \frac{1}{\pi}\mathcal{P}\int_{-\infty}^{\infty}\frac{\Sigma''(\epsilon')}{\epsilon' - \epsilon}d\epsilon'. \tag{20}$$

If the self-energy in Eq. (19) is used, then $\Sigma'(\epsilon)$ diverges at large $|\epsilon|$ due to the $|\epsilon|$ dependence of the density of states. This divergence is unphysical, since the phonons are coupled to π electrons which have a finite bandwidth. Thus the divergence needs to be regularized with a cutoff compatible with the finite-bandwidth requirement, as is customary in graphene (see, for example, Refs. 8, 15, and 16). We adopted the following regularization:

$$\Sigma''_{\text{reg}}(\epsilon) = \begin{cases} \Sigma''(\epsilon) & \text{if } |\epsilon| < \epsilon_M, \\ \Sigma''(\epsilon_M) & \text{if } \epsilon_M < |\epsilon|. \end{cases} \tag{21}$$

With this assumption, the calculation of the integral in Eq. (20) leads to

$$\begin{aligned}\Sigma'(\epsilon) = &- N_\sigma(\epsilon_f)\langle g^2_{\mathbf{\Gamma}}\rangle\left((\epsilon+\hbar\omega_{\mathbf{\Gamma}E_{2g}})[-2\ln|\epsilon+\hbar\omega_{\mathbf{\Gamma}E_{2g}}| + \ln|(\epsilon_M+\epsilon)(\epsilon_f-\hbar\omega_{\mathbf{\Gamma}E_{2g}}-\epsilon)|] + (\epsilon-\hbar\omega_{\mathbf{\Gamma}E_{2g}})\ln\left|\frac{\epsilon_M-\epsilon}{\epsilon_f+\hbar\omega_{\mathbf{\Gamma}E_{2g}}-\epsilon}\right|\right)\\
&- \frac{N_\sigma(\epsilon_f)\langle g^2_{\mathbf{K}}\rangle}{2}\left((\epsilon+\hbar\omega_{\mathbf{K}A_{1'}})[-2\ln|\epsilon+\hbar\omega_{\mathbf{K}A_{1'}}| + \ln|(\epsilon_M+\epsilon)(\epsilon_f-\hbar\omega_{\mathbf{K}A_{1'}}-\epsilon)|] + (\epsilon-\hbar\omega_{\mathbf{K}A_{1'}})\ln\left|\frac{\epsilon_M-\epsilon}{\epsilon_f+\hbar\omega_{\mathbf{\Gamma}A_{1'}}-\epsilon}\right|\right)\\
&- N_\sigma(\epsilon_f)\left(\langle g^2_{\mathbf{\Gamma}}\rangle(\epsilon-\hbar\omega_{\mathbf{\Gamma}E_{2g}}) + \frac{\langle g^2_{\mathbf{K}}\rangle}{2}(\epsilon-\hbar\omega_{\mathbf{K}A_{1'}})\right)\times\left(\ln\left|\frac{\epsilon_M+\epsilon}{\epsilon_M-\epsilon}\right|\right).\end{aligned} \tag{22}$$

In practical calculations we verified that the results are unaffected[17] by the choice of ϵ_M in the range of 1–7 eV. The results presented in this work are with $\epsilon_M = 1.5$ eV.

The real part of the electron self-energy is illustrated in Fig. 2 and is compared with the real part obtained from the Kramers-Kronig transformation of $\Sigma''(\omega)$ with a constant density of states.

In ARPES experiments the spectral weight is measured, namely,[18]

$$A(\mathbf{k},\epsilon) = \frac{-2[\Sigma''(\epsilon)+\eta]}{[\epsilon-\epsilon_{\mathbf{k}}-\Sigma'(\epsilon)]^2+[\Sigma''(\epsilon)+\eta]^2}, \tag{23}$$

where we allowed for a small constant imaginary part η to eliminate numerical instabilities. Typically, $\eta = 10^{-4}$ eV

IV. RESULTS

In this section we consider a Fermi level of $\epsilon_f = 0.4$ eV measured from the Dirac point. Neglecting resolution effects, the spectral function [Eq. (23)] is shown in Fig. 3 (top). The scans presented are fixed photoelectron energy scans (the energy value is given on the left of Fig. 3 top) while the photoelectron momentum is varied (MDC scans). In the MDC scans two kinks are present (compare scans *g* and *h* for the first kink and scans *e* and *d* for the second) in both the spectral-weight maximum position and linewidth.

The behavior of the MDC maximum position as a function of energy and momentum is illustrated in Fig. 3 (bottom). The lower-energy kink corresponds to the twofold-degenerate E_{2g} mode, while the higher-energy one corresponds to the A'_1 mode.

The behavior of the MDC linewidth [half width at half maximum (HWHM)] as a function of energy is shown in Fig. 4. Notice that, in the absence of resolution effects, the linewidth is equal to $-\beta\Sigma''(\epsilon)$. The behavior of the linewidth is compared with that of the square well model typically used to interpret ARPES data. The differences are negligible at energies larger than −0.2 eV, but they are significant at lower energies and in particular at the Dirac point.

To test the robustness of the phonon features against experimental resolution, we introduce the following convoluted spectral weight:

$$\begin{aligned}A_{\text{expt}}(\mathbf{k},\epsilon) = f(\epsilon)\int_{-\infty}^{\infty}d\epsilon'\int d^3\mathbf{k}'\\ \times A(\mathbf{k}',\epsilon')G_{\eta_\epsilon}(\epsilon'-\epsilon)G_{\eta_{\mathbf{k}}}(\mathbf{k}'-\mathbf{k}),\end{aligned} \tag{24}$$

where $G_{\eta_x}(x)$ is a Gaussian having full width η_x and centered at $x=0$. The Fermi distribution is indicated by

$$f(\epsilon) = \frac{1}{\exp[(\epsilon-\epsilon_f)/k_BT]+1}. \tag{25}$$

This form of the experimental resolution assumes that the momentum and energy resolutions are decoupled.

We chose $\eta_\epsilon = 25$ meV and $\eta_{\mathbf{k}} = 0.01$ Å^{-1}, as in recent ARPES experiments.[6,9] The maximum position in $A_{\text{expt}}(\mathbf{k},\epsilon)$ is plotted in Fig. 5.

As can be seen, the experimental resolution substantially smears out the two kinks so that a very weak kink is visible at −0.2 eV while the second one is almost invisible. The kink is substantially smaller than that detected in experiments.[6] The mass enhancement parameter is defined as[12,13]

$$\lambda = -\left.\frac{\partial\Sigma'(\epsilon)}{\partial\epsilon}\right|_{\epsilon=\epsilon_f}. \tag{26}$$

Linearizing $\Sigma'(\epsilon) \approx -\lambda\epsilon$, the spectral weight becomes (for $\eta = 0$)

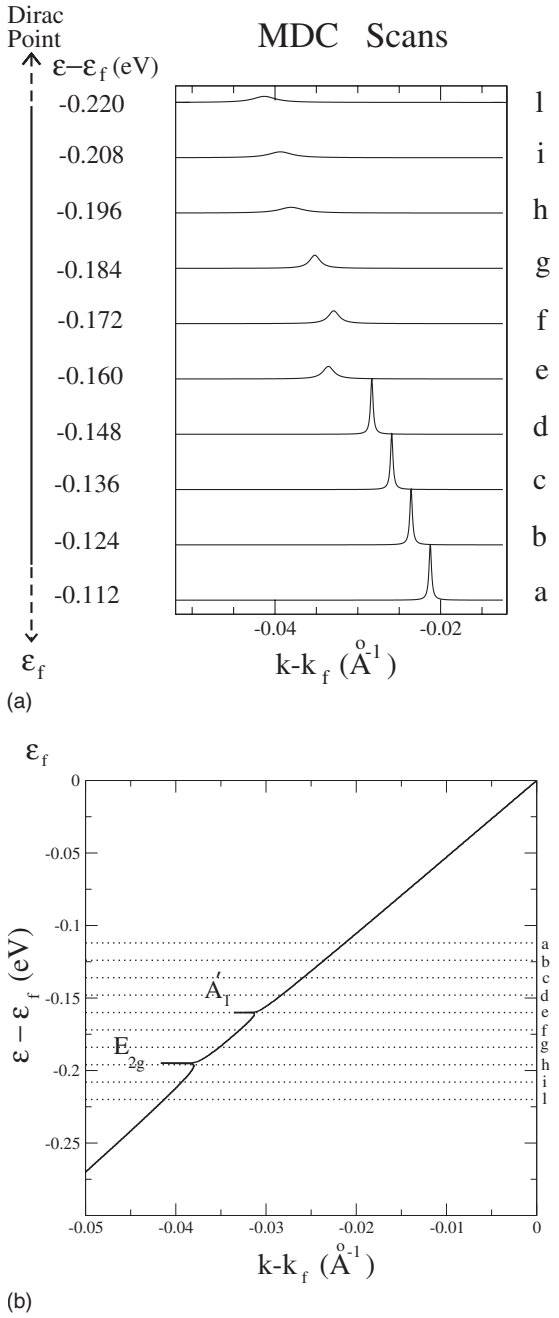

FIG. 3. MDC scans for different energies (top) and ARPES maximum position as a function of energy and momentum (bottom). The Fermi level is ϵ_f=0.4 eV; the experimental resolution is not included in the calculation. A 1 meV broadening is used for illustration purposes.

$$A(\mathbf{k},\epsilon) \approx \frac{-2\Sigma''(\epsilon)Z^2}{(\epsilon - Z\epsilon_{\mathbf{k}})^2 + [\Sigma''(\epsilon)Z]^2}, \tag{27}$$

where

$$Z = \frac{1}{1+\lambda} \tag{28}$$

is the quasiparticle weight. From Eq. (27) one sees that the quasiparticle state has quasiparticle energy $Z\epsilon_{\mathbf{k}}$ and linewidth

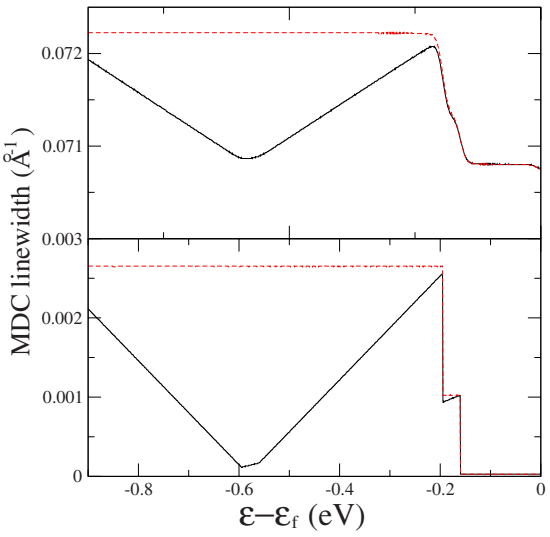

FIG. 4. (Color online) MDC linewidth (HWHM) of the two models' self-energies. The curve in the upper panel is obtained using a finite resolution, while that in the lower one is without resolution effects. In the absence of resolution effects, the linewidth is equal to $-\beta\Sigma''(\epsilon)$ (see Fig. 1). The Fermi level is ϵ_f=0.4 eV.

$\Sigma''(\epsilon)Z/2$. In graphene the bare bands are linear, with $\epsilon_k = \beta k$, so that the maximum position in the spectral weight at energies higher than the kink is given by the relation

$$\epsilon_{\mathbf{k}}^{\max} = \frac{\beta k}{1+\lambda}. \tag{29}$$

Assuming linear renormalized bands, $\epsilon_{\mathbf{k}} = \beta_{\mathrm{ph}} k$, for energies larger than the kink then the following expression for λ is obtained:

$$\lambda = \frac{\beta}{\beta_{\mathrm{ph}}} - 1. \tag{30}$$

In experiments, β_{ph} is obtained from a linear fit at energies higher than the kink but enough below ϵ_f so that the effects

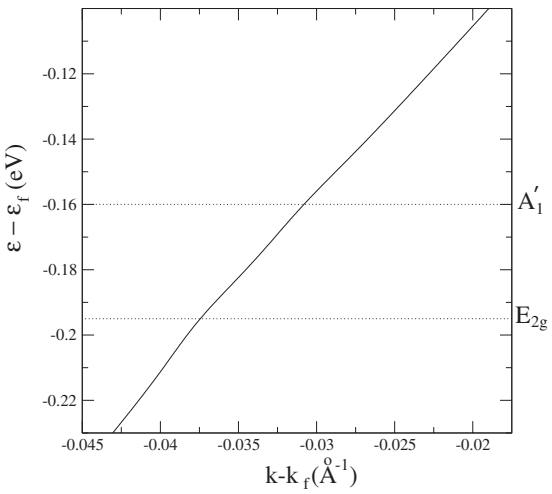

FIG. 5. Position of the maximum in MDC curves using a finite resolution. The Fermi level is ϵ_f=0.4 eV.

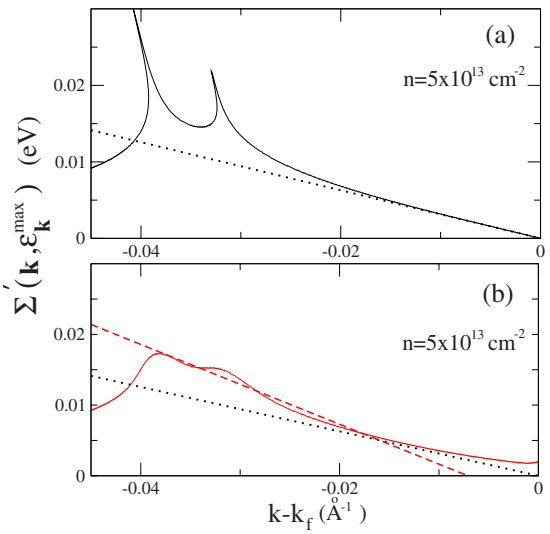

FIG. 6. (Color online) Shift of the maximum in MDC curves due to the electron-phonon coupling, $\Sigma'(\mathbf{k},\epsilon_{\mathbf{k}}^{\max})$, with (b) and without (a) the experimental resolution. The derivative of the curve at k_f in the absence of a finite resolution is shown as a dotted black line in (a) and (b). The dashed red line is a linear fit to $\Sigma'(\mathbf{k},\epsilon_{\mathbf{k}}^{\max})$ in the presence of a finite resolution in the k range $-0.195<k-k_f<-0.04$ eV/β.

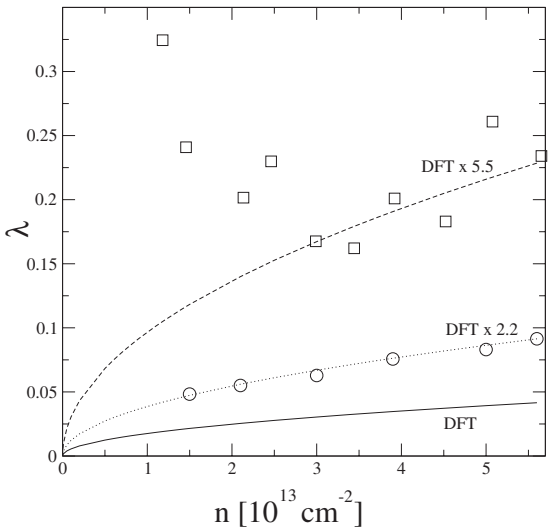

FIG. 7. Electron-phonon coupling in electron-doped graphene. The continuous line labeled DFT refers to Eq. (15), the empty squares are experimental data from Fig. 5 in Ref. 9, while the empty circles represents the apparent electron-phonon coupling extracted from fits to the calculated ARPES spectra using Eq. (30) and including resolution effects. The curves DFT×5.5 and DFT×2.2 indicate Eq. (30) multiplied by the prefactors 5.5 and 2.2, respectively.

of the Fermi function in Eq. (24) are absent. In contrast, the value of β is not directly measurable in experiments, since it is not possible to switch off the electron-phonon interaction. If $\Sigma''(\omega)$ is well described by a square model (which is not the case for graphene), the real part of the self-energy tends to zero at large energies below the kink (see Fig. 2, lower panel, red dashed line), and the slope of the renormalized bands tends to that of the bare bands. On the contrary, if the more realistic model for $\Sigma''(\omega)$ is used, then the slope of the bands below the kink is also renormalized to a value $\tilde{\beta}$ (Fig. 2, lower panel, black continuous line). In ARPES experiments on graphene, the square model is assumed to be valid, and thus the slope of the bare bands is obtained from a linear fit to the maximum position in the MDC curves at energies below the kink (in the range -0.7 to -0.25 eV from the Fermi level). This actually measures $\tilde{\beta}$ and not β.

An additional problem in obtaining λ from experiments is the finite experimental resolution, which affects the value of β_{ph}. In Fig. 6 we plot the shift of the maximum in the MDC curves due to the electron-phonon coupling, $\Sigma'(\mathbf{k},\epsilon_{\mathbf{k}}^{\max})$, with (b) and without (a) the experimental resolution. In the absence of experimental resolution we extract the derivative of the curve at k_f (dotted black line), while in the presence of a finite resolution we perform a linear fit (dashed red line) in the range used in experiments ($-0.195<\epsilon-\epsilon_f<-0.04$ eV). The values of β_{ph} extracted in these two ways differ by a factor of 1.8. Indeed, the nonlinearity of the renormalized band above the kink, when convoluted with a finite resolution, results in a quasilinear behavior with an "apparent" enhanced electron-phonon coupling.

In Fig. 7 we compare the values of the electron-phonon coupling determined in experiments[9] with the DFT values obtained by Eq. (15) and that obtained from the equation $\lambda=\tilde{\beta}/\beta_{\text{ph}}-1$ where both $\tilde{\beta}$ and β_{ph} are fitted from theoretical MDC taking into account experimental resolution.

Notice that the three determinations of λ are in clear disagreement, even if the disagreement between experimental data and Eq. (15) is significantly reduced by resolution effects. A possible source of error in the DFT results is the underestimation of the slope β of the bare bands; the Fermi velocity extracted from experiments[5] is slightly larger (10–20%) than that calculated theoretically using density functional theory. However, using the experimental β, the disagreement between the ARPES-measured λ and the theoretical values gets even worse. Indeed, assuming that the DFT electron-phonon matrix elements are correct, λ scales as $\sqrt{n}\beta^{-1}$ [Eq. (30)]; therefore an underestimation of β results in an overestimation of λ.

For the reasons explained in this section, we believe that the determination of λ using Eq. (30) is affected by large errors. The errors are due to the difficulties in the determination of both β_{ph} and the slope of the bare bands.

V. ELECTRON RELAXATION TIMES IN GRAPHITE AND GRAPHENE

A. Electron-doped graphene

It is interesting to compare the ARPES-measured self-energy imaginary part with that detected by alternative experimental techniques. In electron-doped graphene, the electron relaxation time has been determined experimentally by conductivity and mobility data[19] and by angular-resolved photoemission measurements.[6] The mobility measurement detects the scattering time of electrons at energies $|\epsilon-\epsilon_f|$

$<k_BT$, where k_B is the Boltzmann constant and T is the temperature at which the experiment is performed ($T\approx 300$ K). As shown in Appendix B, this leads to an electron scattering time of the order of

$$\tau = 0.35 \text{ ps} \quad \text{(from mobility)} \tag{31}$$

for $\epsilon_f > 0.2$ eV. Since the Debye temperature of the optical phonon in graphene is much larger then 300 K, the scattering in the mobility measurements is mainly due to defects and acoustic phonons.

ARPES measures the electron self-energy at photoemitted electron energies ϵ. The imaginary part of the electron self-energy is related to the electron scattering time by the relation $\tau(\epsilon)=\hbar/[2\Sigma''(\epsilon)]$. From the data in Refs. 6 and 7 for $|\epsilon-\epsilon_f|\approx k_BT$, we obtain

$$\tau \approx 3.5 \text{ fs} \quad \text{(from ARPES)}, \tag{32}$$

which is two orders of magnitude smaller than Eq. (31).

B. Graphite

In graphite the electron scattering time has been measured by two different experimental techniques, (i) femtosecond time-resolved spectroscopy[20] and (ii) ARPES.

From femtosecond time-resolved spectroscopy,[20]

$$\tau \approx \begin{cases} 0.2 \text{ ps} & \text{for } |\epsilon-\epsilon_f| = 0.25 \text{ eV} \\ 0.1 \text{ ps} & \text{for } |\epsilon-\epsilon_f| = 0.50 \text{ eV} \end{cases} \quad \text{(from femtosecond time-resolved spectroscopy)}. \tag{33}$$

Similar to what happens in graphene, ARPES measurements[4,5,21,22] lead to a relaxation time two orders of magnitude smaller than that obtained from the femtosecond photoemission spectroscopy. For example, from the measured ARPES linewidth in Ref. 22 [see Fig. 10(c)], we obtain

$$\tau \approx \begin{cases} 4.7 \text{ fs} & \text{for } |\epsilon-\epsilon_f| = 0.25 \text{ eV} \\ 3.4 \text{ fs} & \text{for } |\epsilon-\epsilon_f| = 0.50 \text{ eV} \end{cases} \quad \text{(from ARPES)}. \tag{34}$$

VI. CONCLUSIONS

In this work we calculated the electron-phonon coupling parameter and the electron-phonon coupling contribution to the electron self-energy in doped graphene. From the electron self-energy we obtained the spectral-weight function and the ARPES spectra.

The ARPES spectra as a function of momentum and energy displays two kinks. The kinks are at energies $\epsilon-\epsilon_f\approx -0.195$ and -0.16 eV, where ϵ_f is the Fermi level. The two kinks are due to coupling to the twofold-degenerate E_{2g} mode and to the A_1' mode, respectively. The MDC linewidth as a function of energy is discontinuous (jumps) at the E_{2g} and A_1' phonon energies.

Comparing the calculated electron-phonon coupling with that extracted from ARPES experiments, we found that, for large enough electron doping, the latter is roughly a factor of 5.5 larger than the former, as suggested in Ref. 9. We partially solved this contradiction by including finite-resolution effects. Indeed, in experiments the electron-phonon coupling is determined from the ratio of the electron velocities at higher and lower energies with respect to the kink. The velocities are obtained from the slopes of the maximum position of the ARPES spectra as a function of energy and momentum. We find that the slope above the kink is substantially affected by the presence of a finite resolution and the extracted values of the electron-phonon coupling are ≈ 2.2 larger than is obtained without any resolution effect. Thus when comparing calculated spectra with the inclusion of finite-resolution effects to ARPES experiments,[6,9] we remark that the measured electron-phonon coupling is still a factor of 2.5 larger than the calculated one.[10] Thus this work shows once more[23] the importance of including resolution effects to correctly describe ARPES data.

Finally, from the imaginary part of the electron self-energy, we obtain the electron relaxation time. The calculated electron relaxation time is in good agreement with mobility data on electron-doped graphene and is of the same order of magnitude as the electron relaxation time obtained from conductivity and femtosecond time-resolved spectroscopy measurements in graphite. However, this is in strong disagreement with ARPES measurements, the ARPES relaxation times, in both graphene and graphite, being almost two orders of magnitude smaller. This discrepancy essentially reflects the disagreement in the measured and calculated electron-phonon coupling. The aforementioned disagreement in the electron self-energies is even more surprising when considering that previous DFT calculations of the phonon self-energy in graphene, graphite, and nanotubes were found to be in perfect agreement with experimental data concerning phonon dispersion and phonon lifetimes.[24–26] Since the electron and phonon self-energies involve the same vertex, and thus the same matrix elements, a good agreement would be expected even for the electron self-energies too.

Recently, we became aware of two similar works on the subject.[15,27] The results, based on first-principles DFT calculations, presented in Ref. 27 are very similar to ours. Instead, the λ values used in Ref. 15 are twice the DFT values found here or in Ref. 27.

ACKNOWLEDGMENTS

We acknowledge illuminating discussions with Olle Gunnarsson, Eli Rotenberg, Aaron Bostwick, Jessica McChesney, and Shuyun Zhou. Calculations were performed at the IDRIS supercomputing center (Project No. 071202).

APPENDIX A: EVALUATION OF THE INTEGRAL $J_{\mathbf{K}+\tilde{\mathbf{q}}}$

In Eq. (12), $\theta_{\tilde{\mathbf{k}},\tilde{\mathbf{k}}+\tilde{\mathbf{q}}}=2\theta_{\tilde{\mathbf{k}}\tilde{\mathbf{q}}}-\pi$, so that $1-\cos(\theta_{\tilde{\mathbf{k}},\tilde{\mathbf{k}}+\tilde{\mathbf{q}}})=2\cos^2(\theta_{\tilde{\mathbf{k}}\tilde{\mathbf{q}}})$ and the integral $J_{\mathbf{K}+\tilde{\mathbf{q}}}$ [see Eq. (13)] can be evaluated as

$$J_{\mathbf{K}+\tilde{\mathbf{q}}} = \int_0^{2\pi} d\theta_{\mathbf{k}\tilde{\mathbf{q}}} \int \frac{d\tilde{k}}{\Omega} 2\tilde{k}\cos^2(\theta_{\mathbf{k}\tilde{\mathbf{q}}})\delta(\beta\tilde{k} - \beta k_f) \times \delta(\beta|\tilde{\mathbf{k}} + \tilde{\mathbf{q}}| - \beta k_f)$$

$$= \frac{2\epsilon_f}{\Omega\beta^3}\int_0^{2\pi} d\theta_{\mathbf{k}\tilde{\mathbf{q}}}\cos^2(\theta_{\mathbf{k}\tilde{\mathbf{q}}}) \times \delta\left(\sqrt{k_f^2 + \tilde{q}^2 + 2\tilde{k}\tilde{q}\cos(\theta_{\mathbf{k}\tilde{\mathbf{q}}})} - k_f\right)$$

$$= \frac{2k_f}{\Omega\beta^2}\sum_{\alpha=1,2}\int_{-1}^{1} d[\cos(\theta_{kq}^{\alpha})]\delta\left(\cos(\theta_{\mathbf{k}\tilde{\mathbf{q}}}^{\alpha}) + \frac{\tilde{q}}{2k_f}\right) \times \frac{\cos^2(\theta_{\mathbf{k}\tilde{\mathbf{q}}}^{\alpha})\sqrt{k_f^2 + \tilde{q}^2 + 2k_f\tilde{q}\cos(\theta_{\mathbf{k}\tilde{\mathbf{q}}}^{\alpha})}}{k_f\tilde{q}|\sin(\theta_{\mathbf{k}\tilde{\mathbf{q}}}^{\alpha})|}$$

$$= \frac{2}{\Omega\beta^2}\frac{\tilde{q}/2k_f}{\sqrt{1 - \tilde{q}^2/4k_f^2}}. \tag{A1}$$

Furthermore, the integral of such a quantity is

$$A = \int_{\mathcal{F}_{\mathbf{K}}(2\epsilon_f)} \frac{d^2\tilde{\mathbf{q}}}{\Omega} J_{\mathbf{K}+\tilde{\mathbf{q}}} = \frac{2}{\Omega^2\beta^2}\int_{\mathcal{F}_{\mathbf{K}}(2\epsilon_f)} d^2\tilde{\mathbf{q}}\frac{q/2k_f}{\sqrt{1 - q^2/4k_f^2}} = \frac{8k_f^2}{\Omega^2\beta^2}\int_0^{2\pi} d\theta\int_0^1 dy\frac{y^2}{\sqrt{1-y^2}}$$

$$= \frac{2\pi 8k_f^2}{\Omega^2\beta^2}\left[-\frac{y\sqrt{1-y^2}}{2} + \frac{1}{2}\arcsin(y)\right]_0^1 = \frac{16\pi k_f^2}{\Omega^2\beta^2}\frac{\pi}{4} = \frac{16\pi^2\epsilon_f^2}{\Omega^2\beta^4}\frac{1}{4} = \frac{N_\sigma^2(\epsilon_f)}{4}. \tag{A2}$$

APPENDIX B: FROM MOBILITY TO ELECTRON RELAXATION TIME

The conductivity tensor is[28]

$$\sigma = 2e^2\sum_\nu \int \frac{d^2k}{(2\pi)^2}\tau_\nu(\mathbf{k})\mathbf{v}_\nu(\mathbf{k})\cdot\mathbf{v}_\nu(\mathbf{k})\left(-\frac{\partial f}{\partial\epsilon}\right)_{\epsilon=\epsilon_\nu(\mathbf{k})}. \tag{B1}$$

Equation (B1) should then be divided by 2 since we are interested in only one component of the conductivity tensor. Moreover, we consider only intraband transitions since they are only relevant at low temperature. The graphite bands are linear so that $\epsilon_k = \pm\beta k = \pm\hbar v_f k$ where k measure the distance from the **K** point. At zero temperature, only electrons on the Fermi surface contribute to the integral; thus, assuming a constant relaxation time, one gets

$$\sigma \approx 2e^2\sum_\nu v_f^2\tau\int_{\mathcal{F}_{\mathbf{K}}}\frac{dk\,k}{(2\pi)^2}\int_0^{2\pi} d\theta\,\delta(\epsilon_f - \epsilon_{\mathbf{k}\nu})$$

$$= e^2\sum_\nu \frac{v_f^2\tau}{\hbar^2 v_f^2}\frac{\epsilon_f}{\pi} = \frac{e^2\tau\epsilon_f}{\hbar^2\pi}, \tag{B2}$$

so that

$$\tau = \frac{\hbar^2\pi\sigma}{e^2\epsilon_f}. \tag{B3}$$

The conductivity can be written as a function of the mobility as $\sigma = ne\mu$, where n is the number of electrons participating in conduction per surface area. Using Eq. (1) in Ref. 25 $n = \epsilon_f^2/(\pi\beta^2)$ and $\sigma = \epsilon_f^2 e\mu/(\pi\beta^2)$. Thus the relaxation time becomes

$$\tau = \frac{\hbar^2\pi n\mu}{e\epsilon_f} = \frac{\hbar^2\epsilon_f\mu}{e\beta^2}, \tag{B4}$$

where ϵ_f is expressed in eV and μ in $\mathrm{cm}^2/\mathrm{V\,s}$. Expressing the mobility in $\mathrm{m}^2/\mathrm{V\,s}$ one gets

$$\tau = 1.47\times 10^{-12}\epsilon_f\mu = 1.47\times\epsilon_f\mu\ \mathrm{ps}. \tag{B5}$$

Using the values of Ref. 19 for mobility, one gets at large doping ($\epsilon_f > 0.18$ eV) values of the order of 0.35 ps.

[1] For a recent review, see, e.g., K. S. Novoselov and A. K. Geim, Nat. Mater. **6**, 183 (2007).
[2] W. A. Harrison, *Electronic Structure and the Properties of Solids* (Dover, New York, 1989), p. 95, Exercise 3-3.
[3] P. R. Wallace, Phys. Rev. **71**, 622 (1947).
[4] S. Y. Zhou, G.-H. Gweon, C. D. Spataru, J. Graf, D.-H. Lee, Steven G. Louie, and A. Lanzara, Phys. Rev. B **71**, 161403(R) (2005).
[5] S. Y. Zhou, G.-H. Gweon, J. Graf, A. V. Fedorov, C. D. Spataru, R. D. Diehl, Y. Kopelevich, D.-H. Lee, Steven G. Louie, and A. Lanzara, Nat. Phys. **2**, 595 (2006).
[6] A. Bostwick, T. Ohta, T. Seyller, K. Horn, and E. Rotenberg, Nat.

Phys. **3**, 36 (2007).
[7] S. Y. Zhou (private communication).
[8] E. H. Hwang, B. Y. K. Hu, and S. Das Sarma, arXiv:cond-mat/0612345 (unpublished).
[9] A. Bostwick, T. Ohta, J. L. McChesney, T. Seyller, K. Horn, and E. Rotenberg (unpublished); J. McChesney, A. Bostwick, T. Ohta, T. Seyller, K. Horn, and E. Rotenberg (unpublished).
[10] M. Calandra and F. Mauri, Phys. Rev. Lett. **95**, 237002 (2005). Note that in Eq. (1) of this paper there is an error in the prefactor. The correct prefactor is reported in Eq. (15) of the present work.
[11] S. Piscanec, M. Lazzeri, F. Mauri, A. C. Ferrari, and J. Robertson, Phys. Rev. Lett. **93**, 185503 (2004).
[12] Gerald Mahan, *Many Particle Physics*, 3rd ed. (Kluwer Academic/Plenum, Dordrecht, 2000), p. 136.
[13] G. Grimvall, *The Electron-Phonon Interaction in Metals* (North Holland, Amsterdam, 1981), p. 201.
[14] T. Cuk, D. H. Lu, X. J. Zhou, Z. X. Shen, T. P. Devereaux, and N. Nagaosa, Phys. Status Solidi B **242**, 11 (2005).
[15] Wang-Kong Tse and S. Das Sarma, arXiv:0707.3651 (unpublished).
[16] M. I. Katsnelson, Eur. Phys. J. B **52**, 151 (2006); E. G. Mishchenko, Phys. Rev. Lett. **98**, 216801 (2007); O. Vafek, *ibid.* **98**, 216401 (2007).
[17] At a doping $n=5.6\times10^{13}$ cm^{-2}, the slope of the renormalized bands above (β_{ph}) and below ($\tilde{\beta}$) the kink varies with ϵ_M ranging from 1 to 7 eV by about +1.8% and +2.0%, respectively. Correspondingly, $\lambda=\beta_{\mathrm{ph}}/\tilde{\beta}-1$ is equal to 0.0340 for $\epsilon_M=1$ eV and 0.0356 for $\epsilon_M=7$ eV.
[18] With this definition, the spectral-weight sum rule takes the form $\int_{-\infty}^{+\infty}(d\omega/2\pi)A(\mathbf{k},\omega)=1$.
[19] Y. Zhang, Y. W. Tan, H. L. Stormer, and P. Kim, Nature (London) **438**, 201 (2005).
[20] G. Moos, C. Gahl, R. Fasel, and M. Wolf, T. Hertel, Phys. Rev. Lett. **87**, 267402 (2001).
[21] K. Sugawara, T. Sato, S. Souma, T. Takahashi, and H. Suematsu, Phys. Rev. Lett. **98**, 036801 (2007).
[22] S. Y. Zhou, G.-H. Gweon, and A. Lanzara, Ann. Phys. (N.Y.) **321**, 1730 (2006).
[23] See X. J. Zhou, J. Shi, T. Yoshida, T. Cuk, W. L. Yang, V. Brouet, J. Nakamura, N. Mannella, S. Komiya, Y. Ando, F. Zhou, W. X. Ti, J. W. Xiong, Z. X. Zhao, T. Sasagawa, T. Kakeshita, H. Eisaki, S. Uchida, A. Fujimori, Z. Zhang, E. W. Plummer, R. B. Laughlin, Z. Hussain, and Z.-X. Shen, Phys. Rev. Lett. **95**, 117001 (2005); X. J. Zhou, J. Shi, W. L. Yang, S. Komiya, Y. Ando, W. Plummer, Z. Hussain, and Z.-X. Shen, *ibid.* **96**, 119702 (2006); T. Valla, *ibid.* **96**, 119701 (2006).
[24] S. Pisana, M. Lazzeri, C. Casiraghi, K. S. Novoselov, A. K. Geim, A. C. Ferrari, and F. Mauri, Nat. Mater. **6**, 198 (2007).
[25] M. Lazzeri and F. Mauri, Phys. Rev. Lett. **97**, 266407 (2006).
[26] M. Lazzeri, S. Piscanec, F. Mauri, A. C. Ferrari, and J. Robertson, Phys. Rev. B **73**, 155426 (2006).
[27] Cheol-Hwan Park, Feliciano Giustino, Marvin L. Cohen, and Steven G. Louie, Phys. Rev. Lett. **99**, 086804 (2007).
[28] N. W. Ashcroft and N. D. Mermin, *Solid State Physics* (Holt, Rinehart and Winston, New York, 1976), p. 250, Eq. (13.25).